

Geophysical Research Letters

RESEARCH LETTER

10.1029/2021GL092919

Key Points:

- We perform numerical simulations of the two-phase Navier-Stokes equations to resolve bubble bursting and jet drop production
- We describe the jet drop distribution for a wide range of bubble conditions, with droplet production from 0.5 to 500 microns
- The jet drop distribution from bubbles under breaking waves is compatible with laboratory measurements of drop distribution

Correspondence to:

L. Deike,
ldeike@princeton.edu


Citation:

Berny, A., Popinet, S., Séon, T., & Deike, L. (2021). Statistics of jet drop production. *Geophysical Research Letters*, 48, e2021GL092919. <https://doi.org/10.1029/2021GL092919>

Received 11 FEB 2021

Accepted 19 APR 2021

Statistics of Jet Drop Production

A. Berny^{1,2}, S. Popinet², T. Séon², and L. Deike^{1,3} 

¹Department of Mechanical and Aerospace Engineering, Princeton University, Princeton, NJ, USA, ²Sorbonne Université, CNRS, UMR 7190, Institut Jean le Rond d'Alembert, Paris, France, ³High Meadows Environmental Institute, Princeton University, Princeton, NJ, USA

Abstract Bubbles bursting at the ocean surface are an important source of sea-spray aerosol. We describe jet drop production, from ensembles of high fidelity numerical simulations of bubble bursting, validated against experimental results. The number of jet drops, their size, and velocity are controlled by the ratio of the bubble size, R_b , and the visco-capillary length, $l_\mu = \rho_w \gamma R_b / \mu_w^2$, where γ is the surface tension, ρ_w , μ_w the water density and viscosity. The mean drop size follows $\langle r_d \rangle \propto (R_b / l_\mu)^{5/4}$ and the ejected number of drops $n \propto (R_b / l_\mu)^{-1/3}$, accounting for temperature variations. We confirm that submicrons jet drops are produced by bubbles in the 10–40 microns range. We compute the distribution of jet drops formed by a range of bubbles present under a breaking wave which compares well against laboratory experiments. We discuss the applicability of the proposed formulation in the context of sea spray generation function.

Plain Language Summary Bubbles bursting at the ocean surface have long been recognized as an important source of sea spray aerosols. However, the description of sea spray production remains elusive in parts due to the large range of scales involved, from bubble bursting at the ocean surface to large scale breaking waves. We discuss the range of droplets that can be formed by bubble bursting, for bubble sizes typical of ocean conditions. We show that jet drops can have sizes from 0.5 to 500 microns, and propose theoretical relationships to describe their size and number, as a function of the bubble size, as well as water temperature and salinity. The results compare very well to laboratory experiments, and pave the way toward mechanistic formulation of sea spray, to be used in atmospheric and climate models.

1. Introduction

Knowledge of the size production flux of primary ocean spray droplets and aerosol particles and its dependence on meteorological and environmental variables is necessary for modeling cloud microphysical properties and the influence of aerosol on radiative processes (Bertram et al., 2018; de Leeuw et al., 2011; Quinn et al., 2015). Biases and uncertainties in predicting sea spray aerosols are related to a lack of fundamental understanding in the production processes of aerosols, and the large range of scales involved going from wave statistics at O (1 km–1 m), to the breaking dynamics at O (1–10 m), air bubble entrainment and bursting at O (microns–mm), which directly impacts our ability to perform weather prediction and earth system modeling (Deike & Melville, 2018; Deike et al., 2017; de Leeuw et al., 2011). Ocean spray is composed of small liquid droplets formed through two main pathways (Veron, 2015): the spume drops, produced from the tearing of breaking wave crests by strong winds (Ortiz-Suslow et al., 2016; Troitskaya et al., 2018; Veron et al., 2012) and bubble bursting, itself decomposed into the film and jet drops production (Cipriano et al., 1983; Ghabache et al., 2014; Lhuissier & Villermaux, 2012; Spiel, 1997). These droplets transport water, heat, dissolved gases, salts, surfactants, and biological materials between the ocean and the atmosphere and these air-sea fluxes are dependent on the drop size distributions (Mueller & Veron, 2014; Peng & Richter, 2020), while their chemical composition is affected by the production mechanisms (Cochran et al., 2017; Wang et al., 2017).

The characterization of all drops requires a statistical approach, performing ensemble of experiments, or simulations of the same bubble bursting process. We present such statistical description of jet drops being ejected by bursting bubbles, including the mean number and size of jet drops being ejected, as well as their size distribution, controlled by the bubble size and water physical properties. This yields simple relationships for the resulting jet drops generated by a typical bubble size distribution under a breaking wave.

The production of droplets due to bubbles bursting at the surface of a liquid has long been considered as a fundamental mechanism controlling larger scale fluxes between the liquid and the gas, and its importance on aerosol generation (Cipriano et al., 1983). Blanchard (1954) and Blanchard and Woodcock (1957) measured the size and height of the ejected droplets, and Spiel (1994, 1997) reported on the statistics of number and sizes of the droplets produced by bubble bursting in both salt and tap water. Using high speed cameras (Brasz et al., 2018; Ghabache & Séon, 2016; Ghabache et al., 2014, 2016) have provided detailed experimental data on the size and velocity of the first droplet. These experimental developments on the dynamic of single bubble bursting have been accompanied by progresses in theoretical and computational description. Duchemin et al. (2002) presented the first numerical simulation of the axisymmetric bursting of a single bubble solving for the two-phase Navier-Stokes equations. They demonstrated that the main controlling parameter of the speed and size of the first ejected droplet is given by the ratio of the bursting bubble size, R_b , and the visco-capillary length $l_\mu = \mu_w^2 / (\rho_w \gamma)$, where μ_w is the water viscosity, ρ_w the water density, and γ the surface tension. This ratio is called the Laplace number:

$$\text{La} = \frac{R_b}{l_\mu} = \frac{\rho_w \gamma R_b}{\mu_w^2}. \quad (1)$$

Duchemin et al. (2002) showed that there exists an optimal value $\frac{R_b}{l_\mu} \approx 1000$, (between $R_b = 10$ and 20 microns in salt water at 20°C) for which the capillary focusing is the most efficient and leads to the ejection of very fast and small droplets (several tens of m/s for air in water, and drops of O [1 μm]). Deike et al. (2018), Brasz et al. (2018), and Lai et al. (2018) demonstrated the universal behavior of the first ejected droplet size and velocity, for a range of Laplace numbers from 900 to 100,000, which correspond to the range of existence of jet drops in water (10 microns–3 mm at 20°C). The experimental and numerical results were used by Gañán-Calvo (2017) to propose scaling laws able to describe the size r_{d1} and velocity V of the first droplet, based on the inertio-capillary focusing of the capillaries along the cavity, and balance of forces during the cavity reversal and jet formation (with $V_\mu = \gamma/l_\mu$):

$$V / V_\mu = k_v \left(\text{La} \left(\text{La}_*^{-1/2} - \text{La}^{-1/2} \right) \right)^{-3/4} \quad (2)$$

$$r_{d1} / l_\mu = k_r \left(\sqrt{\text{La}} \left(\sqrt{\frac{\text{La}}{\text{La}_*}} - 1 \right) \right)^{5/4}. \quad (3)$$

where $\text{La}_* \approx 550$ is the drop ejection threshold, (about 5 μm bubbles in salt water at 20°C), while k_r and k_v are empirical O (1) constants fitted to the data. The asymptotic scaling at high La, for the first drop (or jet) velocity, is then $V/V_\mu \propto \text{La}^{-3/4}$, and for the first drop size, $r_{d1}/l_\mu \propto \text{La}^{5/4}$. It is important to realize that these scaling laws have certain limits. They do not capture the nonmonotonic behavior of drop size and velocity below the optimal Laplace number, but are extremely valuable from a practical point of view. Gordillo and Rodríguez-Rodríguez (2019) and Blanco-Rodríguez and Gordillo (2020) proposed an alternative set of scaling laws based on the ideas of capillary focusing and wavelength selection during the cavity collapse, combined with an inertio-capillary balance. The results are essentially compatible with Equations 4 and 5 at high La, but the treatment of $\text{La} \approx 1,000 \sim \text{La}_c$ is different, and their formula reads

$$V / V_\mu \propto \text{La}^{-1} \left(1 - \left(\sqrt{\frac{\text{La}_c}{\text{La}}} \right)^{1/4} \right)^{-3/2}, \quad (4)$$

$$r_{d1} / l_\mu \propto \text{La} \left(1 - \left(\sqrt{\frac{\text{La}_c}{\text{La}}} \right)^{1/4} \right). \quad (5)$$

The effect of gravity on the bubble shape and selecting the capillaries has been discussed by Ghabache et al. (2014) and Deike et al. (2018) and leads to corrections on the drop size and velocity once $R_b > 0.4l_c$, where $l_c = \sqrt{\gamma / (\Delta\rho g)}$ is the gravity-capillary length, which is 2.7 mm in water at 20°C.

In Berny et al. (2020), we performed axisymmetric numerical simulations of jet drop production by bubble bursting for a wide range of parameters, and extended the analysis to the subsequent droplets to describe the number and size of all jet droplets produced when a cavity collapses. These simulations showed that between 1 and 14 drops are ejected depending on La and $Bo = (R_b / l_c)^2$. The ejection speed of the droplets decreases as the production number increases, while the size of the droplets can be either smaller or larger than the first drop. The results are limited by the sensitivity of the subsequent drop properties to noise in the system, which was already discussed by Spiel (1994, 1997) and Ghabache et al. (2014, 2016), with the existence of bimodal distribution for subsequent drop size distribution.

We introduce variability in the initial conditions through a (axisymmetric) random white noise in the liquid velocity, with a magnitude of 1% of the typical jet velocity. We show that the resulting droplet statistics compares well with the data from Spiel (1994, 1997) (§2). We discuss the drop size distributions for a range of nondimensional control parameters, which accounts for bubble bursting at the ocean surface, considering typical ocean water temperature and their associated density, viscosity, and surface tension (§3). Next, we discuss the resulting drop size distribution when considering the typical size distribution of bubbles under a breaking waves (§4). Finally, we compare the results to existing data set obtained in laboratory settings and discuss the assumptions made in this model, in particular the minimal and maximal bubble size and their implications for aerosol production.

2. Ensemble of Numerical Simulations of Bubble Bursting with Noisy Initial Conditions.

2.1. Numerical Methods

We perform numerical simulations of the two-dimensional axisymmetric, incompressible two-phase Navier-Stokes equations (air and water) with surface tension. We use the free software Basilisk which is based on a spatial adaptive quad-octree grid allowing to save computational time, while resolving the different length scales of the problem (Popinet, 2009; van Hooff et al., 2018). It is based on a momentum conserving scheme and a geometric Volume of Fluid (VOF) method to reconstruct the interfaces (Popinet, 2009, 2018) between the high density liquid (water) and the low density gas (air). These methods have been extensively described and validated in studies exploring complex multiphase flow, in particular wave breaking (Deike et al., 2016; Mostert & Deike, 2020) and bubble bursting (Berny et al., 2020; Deike et al., 2018; Lai et al., 2018).

The physical parameters of the problem are the bubble radius R_b , liquid and air density $\rho_{w, a}$, and dynamic viscosity $\mu_{w, a}$, surface tension γ and gravity g . The initial condition is given by the shape of a bubble at rest below an horizontal interface, obtained by the balance of forces described by the Young-Laplace equation (Ghabache et al., 2014; Lhuissier & Villermaux, 2012; Toba, 1959) which we solve numerically (Berny et al., 2020). The problem is then controlled by the Laplace number, which compares the bubble size to the visco-capillary length $La = R_b/l_\mu$ and the Bond number, which compares the bubble size to the gravity-capillary length $Bo = (R_b / l_c)^2$. Figure 1a shows an example of bubble bursting simulation, displaying cavity collapse, jet formation, and drop production. It is important to note that this approach solves the native two-phase flow equations without any subgrid scale model. We use an adaptive mesh, critical to the success of these simulations as it allows an equivalent resolution of up to 4^{14} grid points (equivalent to 8192^2 and corresponding to 1,638 grid points per bubble diameter, with the smallest grid size in each direction being $\Delta = R_b/3276$). More details of the numerical setup and validation are provided in Deike et al. (2018) and Berny et al. (2020). These simulations resolve all relevant length scale without subgrid scale models with the bursting process assumed axisymmetric, as confirmed by laboratory experiments when the water and air are initially at rest.

The individual simulations are similar to Berny et al. (2020), which analyzed the number, size, and velocity of ejected drops for various La and Bo . The first jet drop properties are summarized in Figures 1b, 1c, and 1d, using numerical data from Berny et al. (2020), Deike et al. (2018), Brasz et al. (2018) and experimental data from Ghabache et al. (2014), Ghabache et al. (2016), Brasz et al. (2018). The existence of jet drops as

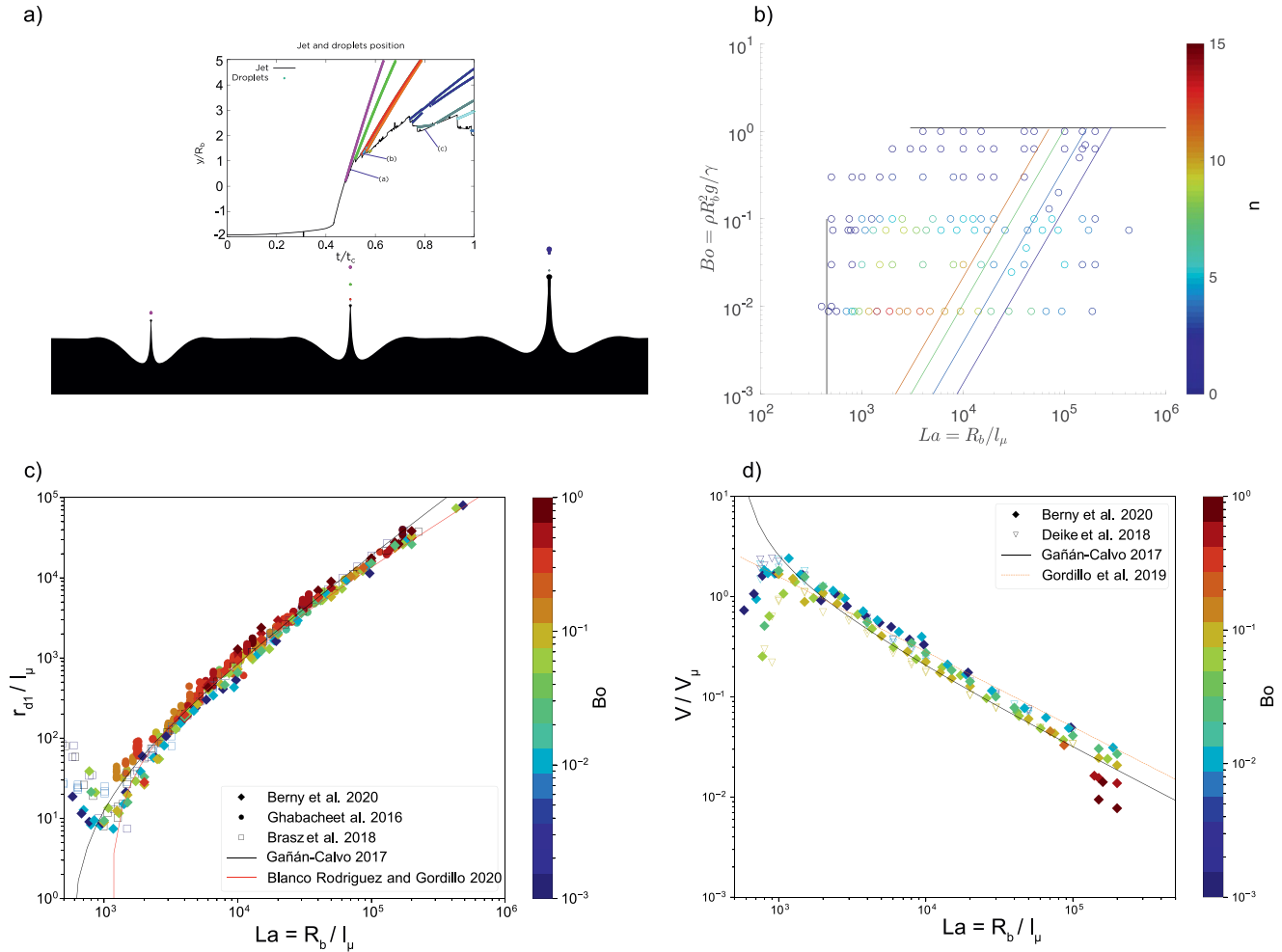


Figure 1. Jet drop dynamics and characteristics. (a) Numerical simulations of the two-phase flow process can be performed, and capture for a given initial cavity all jet drops being produced (Berny et al., 2020). Inset shows the position of the tip of the jet (black) and droplet position (the ejected drop being color coded). (b) Phase diagram of existence of jet drops in terms of controlling parameters, R_b/l_μ and R_b^2/l_c^2 , from Berny et al. (2020). The number of ejected droplet is color coded. The colored lines correspond to salt water conditions at 4, 10, 20, and 28°C. For $R_b^2/l_c^2 > 1$, no jet drops are being produced. (c) The first drop size, normalized by the visco-capillary length, r_{dt}/l_μ , as a function of the normalized bubble size R_b/l_μ . The first drop size can be described by a universal scaling (Equation 3), and all data collapse onto a single curve. Symbols are simulations and laboratory experiments from Ghabache et al. (2016), Brasz et al. (2018), Deike et al. (2018), and Berny et al. (2020). (d) Same data for the jet drop velocity V/V_μ , as a function of R_b/l_μ . Again, all data collapse onto a single curve and can be described by a universal scaling (Equation 2).

a function of La and Bo is shown in Figure 1b together with the number of ejected drops in each conditions (Berny et al., 2020). The first drop size and velocity are shown in Figures 1c and 1d, with excellent agreement between all data sets and with the scalings of Equation 2 and Equation 3. We note the slow-down of the drop velocity due to gravity for $Bo > 0.2$ ($R_b > 0.4l_c$).

In order to obtain a statistical ensemble of simulations for each configuration, that is, for each La , Bo , we seed the water with random white noise of small amplitude. The amplitude of the noise is typically a few percent of the (expected) jet velocity, so that it presents a perturbation to the flow. We verified that the results are not sensitive to the particular form of the random noise imposed on the velocity field, as long as the perturbation is below a few percent of the characteristic ejection velocity.

We perform ensembles of 120 members for each conditions of interest. We consider 10 cases, with the Laplace number going from 1,000 to 250,000, and the associated Bond number in salt water at 28°C (10 μm –3 mm corresponding to $Bo \rightarrow 0$ to $Bo = 1$). For each ensemble, the data collection is as follows: each run is processed individually, and the number, size, and velocity of each ejected drop is measured at

ejection. All the data from a single ensemble are then gathered, leading to the definition of probability of existence and size distribution of each drop. The data set is also analyzed by gathering all runs together to define the ensemble averaged ejected number, drop size, and size distribution.

2.2. Validation of the Jet Drop Statistics Against Experimental Data

We validate our numerical ensemble approach by comparison with the experimental data set from Spiel (1994, 1997), which are the only experimental studies that have considered the statistics of all ejected droplets. We perform ensembles of simulations corresponding to the data set presented by Spiel (1994, 1997) in both tap water and salt water.

The size distribution of each ejected droplet can then be analyzed and compared to the experiments from Spiel (1994, 1997), as shown in Figures 2a–2f with bubble radii going from 350 to 1215 μm , with a water temperature of 28°C. We show the probability of existence of the n th droplet (Figures 2a, 2c and 2e), as well as the distribution of drop size for the first six droplets (Figures 2b, 2d and 2f). The agreement in terms of probability of existence for all three cases (Figures 2a, 2c and 2e) is remarkable, showing that our setup, despite its strong simplification is able to reproduce the mean number of drops ejected by a bursting bubble in the laboratory for salt water conditions. For the smallest bubble (Figures 2a and 2b), the size distribution of the six drops are also very good, the numerical simulations capturing the size and statistics of all cases. The agreement is still reasonable for the two other cases with larger bubble size (Figures 2c and 2d), with a drop size difference between experiment and numerical simulation around 20%, while the simulations are capturing the bimodal distribution of the droplet 2 and 3. Ensembles of simulations were carried out to reproduce the other cases from Spiel (1994); Spiel (1997) and similar agreement was observed, with good agreement in terms of mean number of ejected drop, and reasonable agreement in terms of drop size statistics, with variations of about 20% when considering individual drops reported by Spiel (1994, 1997).

Given the large uncertainties remaining in the sea spray production processes and the relatively small size of the experimental samples, this is deemed reasonable. We conclude that our simulations are capturing the main properties of the ejected jet drops: the first drop size and velocity is very well captured, together with the mean total number of drops for particular conditions, as well as the size of the subsequent droplets. Moreover, our methodology has the advantage of being easy in terms of computations (compared to performing the corresponding more than 1,000 bubble bursting experiments). We should also keep in mind that both the simulation setup and the laboratory experiment in quiescent condition represent an idealization of the bursting bubble process occurring at the surface of the ocean. The cavity collapse occurs over a time scale of ms to s, and the possible influence of the atmospheric or oceanic turbulent boundary layers on the bursting process and jet destabilization have not yet been characterized. The role of the surrounding bubbles, both just below and at the surface also remain to be fully understood.

3. Number, Mean Size and Distribution of Jet Drops for Ocean Water

From the practical point of view of ocean sea spray production, the universal control of the Laplace number, $La = R_b/l_\mu$ on the drop properties (size and velocity) allows to naturally consider variations in temperature and salinity in the ocean, through their influence on the density, viscosity and surface tension.

We analyze the jet drop statistics obtained from the 10 ensembles described above, corresponding to non-dimensional bubble size R_b/l_μ from 1,000 to 2.5×10^5 . As shown in Figure 1b, this range corresponds to bubbles in salt water, from 10 μm to close to the capillary size, 2.7 mm, and cover the full range of jet drop production in ocean water. We consider the ratio R_b/l_μ as the main controlling parameter as the Bo number only plays a role for bubbles close to the capillary size and will mainly serves as upper cut-off of our scaling relationships, with $R_b/l_\mu > \approx 10^5$ corresponding to $Bo \approx 1$ and the limit of jet drop production.

Figure 3a shows the number of droplets ejected as a function of the bubble Laplace number, R_b/l_μ , aggregating numerical data from (Berny et al., 2020), the ensemble performed here, as well as experimental data from Spiel (1994) and Ghabache (2015). The agreement between simulations and experiments is excellent. The total number of drops is about 15 for $R_b/l_\mu = 1,500$ and decreases through an algebraic relationship until $R_b/l_\mu = 10^5$,

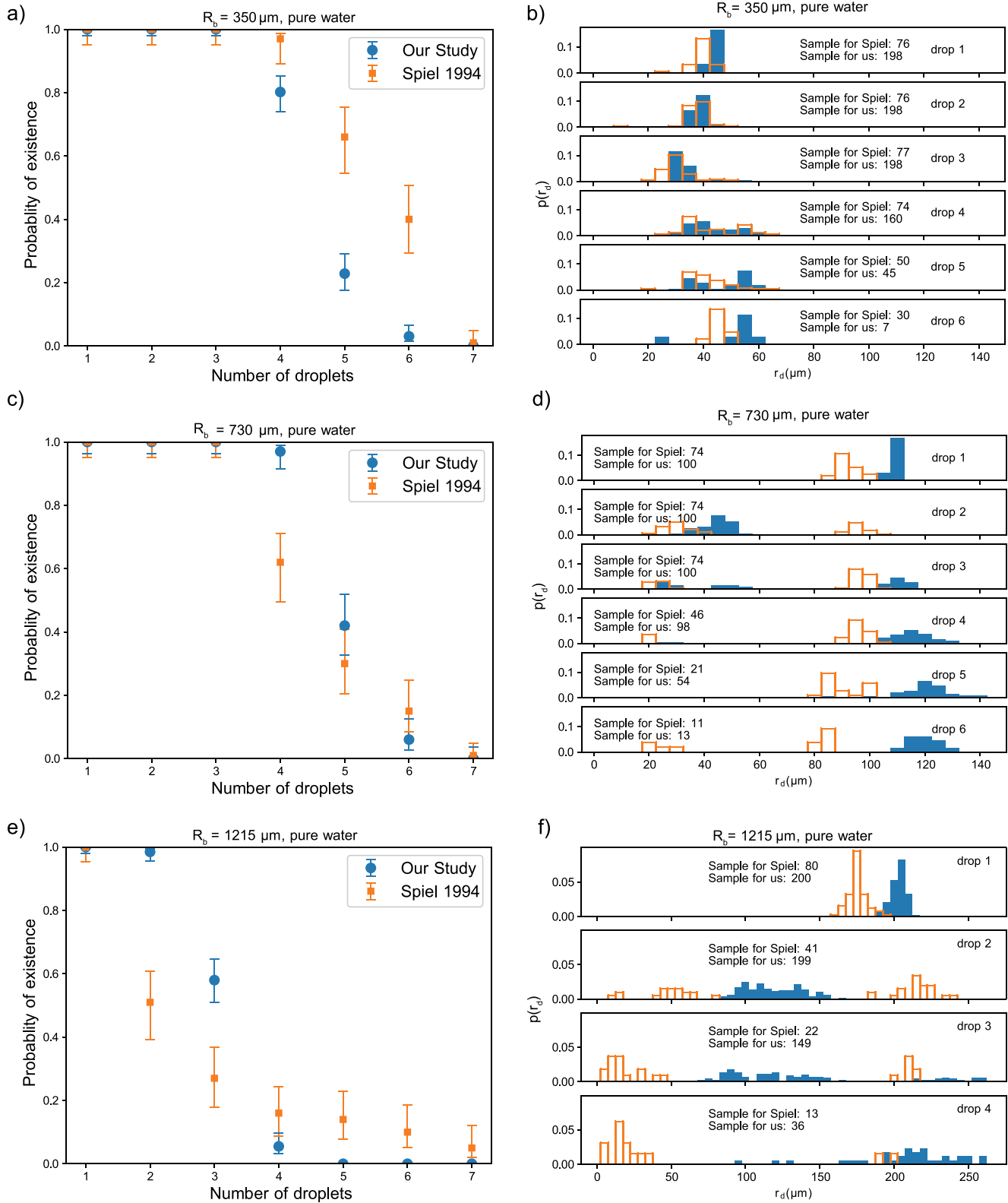


Figure 2. Ensemble of simulations and comparison with experimental data. (a) to (f) Probability of existence of the n th drop from the simulations, compared to Spiel's data, for the $R_b = 354$ (a), 728 (c), and 1213 μm (e) (at 28°C); and probability distribution of the first six drops (b, d, f). Good agreement is observed in terms of probability of existence together with reasonable agreement for the ejected droplet distribution between the simulations and experimental data. This validates our ensembles of simulations to study the statistics of jet drops.

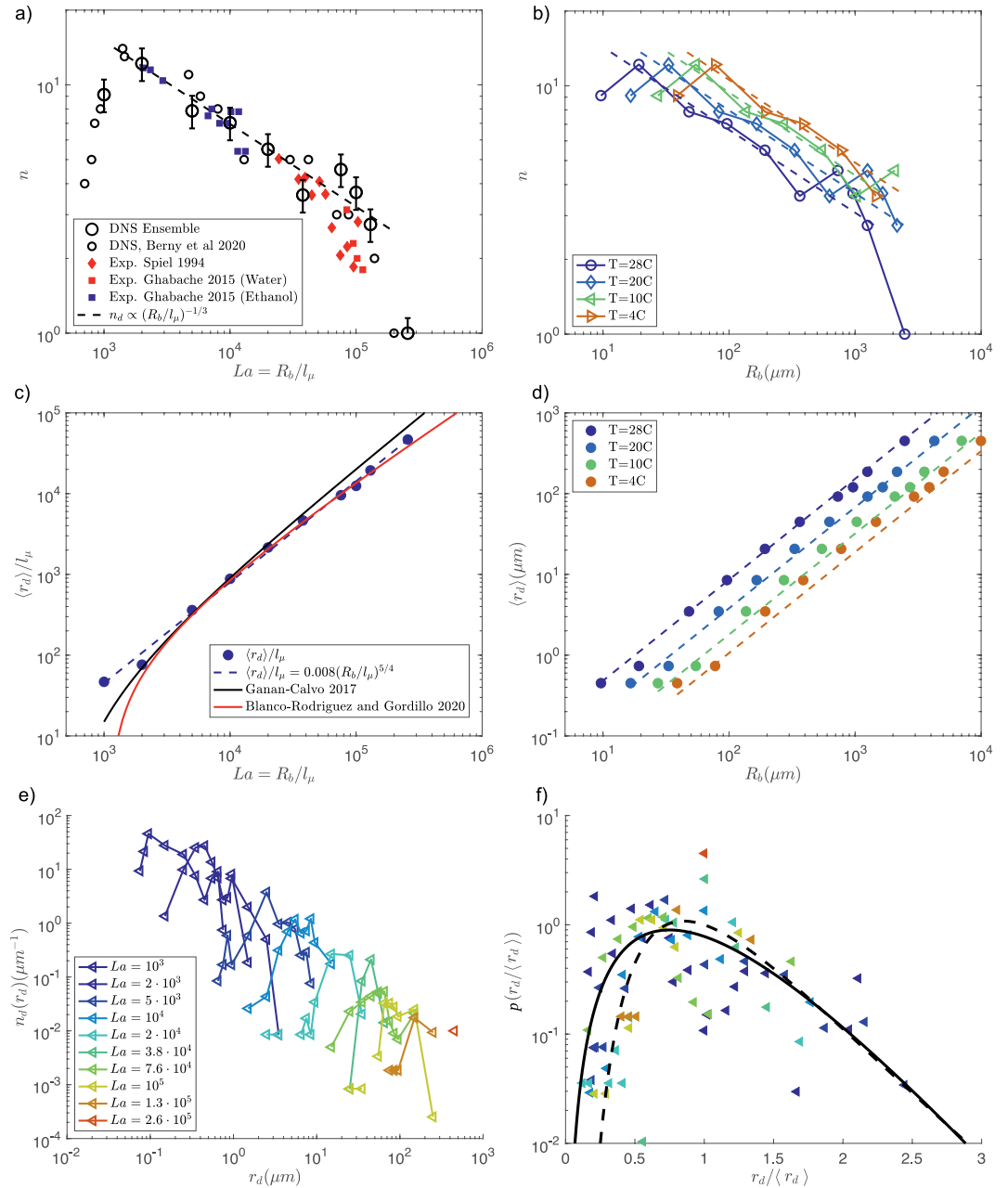


Figure 3. (a) Number of jet drops ejected, as a function of the nondimensional bubble size R_b/l_μ . In (a), we superpose the experimental data from Spiel (1994, 1997) and Ghabache (2015) for water as well as more viscous fluids allowing to explore smaller values of R_b/l_μ (only data with $Bo < 0.05$ are considered to be in the regime, where only R_b/l_μ controls the drop production). Data can be described as $n(R_b) = \chi \left(\frac{R_b}{l_\mu} \right)^{-1/3}$. (b) Numerical data presented as a function of the dimensional R_b for four different water conditions, calculated from (a) using the water properties at these temperatures to compute l_μ , showing that changes in temperature shift the drop production efficiency to larger sizes. (c) Mean ejected drop size $\langle r_d \rangle / l_\mu$ as a function of R_b/l_μ . The data can be described by $\frac{\langle r_d \rangle}{l_\mu} = \eta \left(\frac{R_b}{l_\mu} \right)^{5/4}$, close to the observed scaling for the first drop size. (d) Same data expressed in dimensional units using the water properties at these temperatures to compute l_μ . (e) Size distribution of ejected droplets obtained for the 10 ensembles considered, using l_μ at $T = 28^\circ\text{C}$, so that bubble radii vary from 10 to 2,400 μm . The distribution of ejected droplet size varies from 0.1 to 100 μm . (f) Normalized distributions, with a Gamma distribution of order 4 superimposed (solid black line) and a log-normal distribution (dashed black line).

$$n(R_b) = \chi \left(\frac{R_b}{l_\mu} \right)^{-1/3}, \quad (6)$$

with $\chi = 145$ a nondimensional parameter adjusted to the data. For $R_b/l_\mu > 10^5$, a sharp decrease is observed, with one drop produced at $R_b/l_\mu = 2 \times 10^5$ and no drop above. This is related to the effect of gravity for large bubbles and corresponds to $R_b/l_c = 1$, or $R_b \approx 2.7$ mm, above which gravity prevents drop formation, as illustrated in Figure 1b.

The relationship, Equation 6, can be used to compute the number of drops ejected as a function of the bubble size for given water properties, mainly controlled by salinity and temperature in the ocean. An example of the resulting curves is shown in Figure 3b, where we have considered l_μ for salt water at temperatures of 4°C–28°C. The water temperature shifts the maximum number of drops ejected from about 20 μm at higher temperature to about 100 μm at lower temperature, due to the increase in water viscosity when the temperature is decreased. The cut-off visible in Figure 3b corresponds to the effect of gravity preventing drop ejection for $R_b/l_c > 1$.

Figure 3c shows the first moment of the drop size distribution, the mean droplet size $\langle r_d \rangle = \int r_d n_d(r_d) dr_d$ as a function of the bubble radius R_b/l_μ , together with the scaling relationship (Equations 3 and 5) of the first drop (shown in Figure 1). The mean droplet size increases with the bubble size, and follows closely the scaling observed for the first drop. The scaling can be simplified and for the full range of nondimensional bubble sizes, $900 < R_b/l_\mu < 3 \times 10^5$, can be written as,

$$\frac{\langle r_d \rangle}{l_\mu} = \eta \left(\frac{R_b}{l_\mu} \right)^{5/4}, \quad (7)$$

with $\eta = 0.008$ a nondimensional coefficient adjusted to the data.

Figure 3d shows the same data for temperatures between 4°C and 28°C, which illustrates that in the range of production, larger drops will be produced at lower temperatures, as a consequence of the increased viscosity.

Figure 3e shows the corresponding size distribution of ejected drops, for the 10 ensembles. For simplicity, we consider here the dimensional variables for the 28°C configuration, so that bubble sizes range from 10 μm to 2.5 mm. We write the size distribution $n_d(r_d) = n(R_b)p(r_d, R_b)$, where $n(R_b)$ is the total number of drops ejected for a bubble of size R_b (shown in Figure 3b, $T = 28^\circ\text{C}$) and $p(r_d, R_b)$ is the (normalized) probability distribution function of drop size ejected by the bubble of size R_b . As already discussed, we observe that smaller drops are generated by smaller bubbles, while the distribution appears as skewed exponentials, as a consequence of the jet fragmentation process.

Following the work of Villermaux (2020) on drop formation by fragmentation and Lhuissier and Villermaux (2012) on film drop production by bubble bursting, we seek to represent the drop size distribution of each ensemble by a Gamma distribution, which is a two-parameter distribution controlled by the mean drop size $\langle r_d \rangle$ and its order m , which in the fragmentation context correspond to the rugosity of the jet before fragmentation:

$$\mathcal{P}(r_d / \langle r_d \rangle) = \frac{m^m}{\Gamma(m)} \left(\frac{r_d}{\langle r_d \rangle} \right)^{m-1} e^{-m \frac{r_d}{\langle r_d \rangle}} \quad (8)$$

Figure 3f shows the drop size distribution $p(r_d/\langle r_d \rangle, R_b)$ as a function of $r_d/\langle r_d \rangle$ and that our data can be relatively well described by a Gamma distribution, here $m = 4$ (solid line). This statement is more accurate for smaller bubbles with production of O(10) drops, where the fragmentation scenario is more accurate, while for larger bubbles with O(1) drop being produced, the process is more deterministic, with the drop size selected by the cavity collapse and jet dynamics, and the distribution resulting from the large ensemble is narrower. Note that our data set remains relatively limited in terms of statistical convergence and we do not try to demonstrate that the Gamma distribution is a better statistical model than other options that

could have been considered to represent the jet drop distribution, such as a log-normal distribution (dashed line) which is indicated in Figure 3f and also describes the data. The choice of the Gamma distribution is justified by analytical integrability with bubble size distribution described as power laws in the next section.

4. Application to the Distribution of Jet Drops Generated by a Distribution of Bursting Bubbles Characteristic of a Breaking Wave

Having characterized the drop size distributions for various bubble sizes, we aim to apply the proposed scalings to a canonical bubble size distribution generated by a breaking wave. The bubble size distribution $q(R_b)$ under a breaking wave has been studied by generating breaking waves in laboratory settings (Blenkinsopp & Chaplin, 2010; Deane & Stokes, 2002; Prather et al., 2013; Rojas & Loewen, 2007), as well as through numerical studies (Deike et al., 2016; Mostert et al., 2021). It is usually described by two scalings, separated by the Hinze scale (Hinze, 1955; Rivière et al., 2021), which compares the action of surface tension and turbulence and corresponds to the critical size below which bubbles do not break under the water turbulence, $r_H = C(\gamma / \rho)^{3/5} \varepsilon^{-2/5}$, where ε is the water side turbulence dissipation rate, C an order 1 constant, leading to $r_H \approx 1\text{--}2$ mm in typical conditions. From the discussion above, jet drop production is mainly controlled by bubbles below the Hinze scale. For bubbles larger than the Hinze scale, experiments and simulations support $q(R_b) \propto R_b^{-10/3}$, which can be explained by a turbulent breakup cascade argument (Garrett et al., 2000). For bubbles below the Hinze scale, the bubble size distribution can be described by (Deane & Stokes, 2002; Mostert et al., 2021; Prather et al., 2013; Rivière et al., 2021)

$$q(R_b) \propto R_b^{-3/2}. \quad (9)$$

Experimental measurements of drops produced by a bubble plume characteristic of the bubble population under a breaking wave have been performed by various authors. We consider the recent experiments from Prather et al. (2013) and Erinin et al. (2019) which have measured the drop size distribution resulting from the bursting of bubbles with a bubble bulk size distribution comparable to $q(R_b) \propto R_b^{-3/2}$.

Prather et al. (2013) (see also Quinn et al., 2015) presents measurements of dry aerosol particles between 0.01 and 10 μm , resulting from bubble bursting and are shown in Figure 4 (main). Data are obtained from two sets of experiments where the bubble size distribution is also measured, a breaking wave obtained by linear focusing as well as from a waterfall experiment, with bubble distribution closely matching the $R_b^{-3/2}$ scaling (Prather et al., 2013). The similarity of the drop size distribution demonstrated the importance of the bubble size distribution to understand the resulting drop statistics (Prather et al., 2013). We convert the dry-aerosol diameter into liquid droplet radius by considering the conversion factor $2D_d^{\text{dry}} = 2r_d^{80\%} = r_d$ used in the literature (Lewis & Schwartz, 2004; Tang et al., 1997; Veron, 2015), and keep the absolute count per unit bin size per unit volume from Prather et al. (2013) and Quinn et al. (2015).

Erinin et al. (2019) measured the size distribution of liquid drops from 50 μm to 1 mm, resulting from a breaking wave, and separated their data into stage I at early time, which corresponds to spume drops generated at impact, and stage II at later times which coincides with the bubble plume rising and bursting at the surface. While Erinin et al. (2019) do not report bubble size distribution data, the breaker is obtained by linear focusing in a similar way as Deane and Stokes (2002) and it is reasonable to assume that the bubble size distribution should be comparable. The data from Erinin et al. (2019) are shown in Figure 4 (main).

We aim to compare the predicted drop size distribution with these experimental data. We can write the jet drop size distribution by integrating over all bubble sizes,

$$N_d(r_d) = \int \frac{q(R_b)n(R_b)}{\langle r_d \rangle} p(r_d | \langle r_d \rangle, R_b) dR_b. \quad (10)$$

This assumes that all bubbles will burst and that the bursting process is well captured by the single bubble bursting studies, which are rather strong assumptions that could be modified by considering the bubble plume evolution and measurements of the surface bubble size distribution actually bursting (see the discussion in Neel & Deike, 2021 on collective effects).

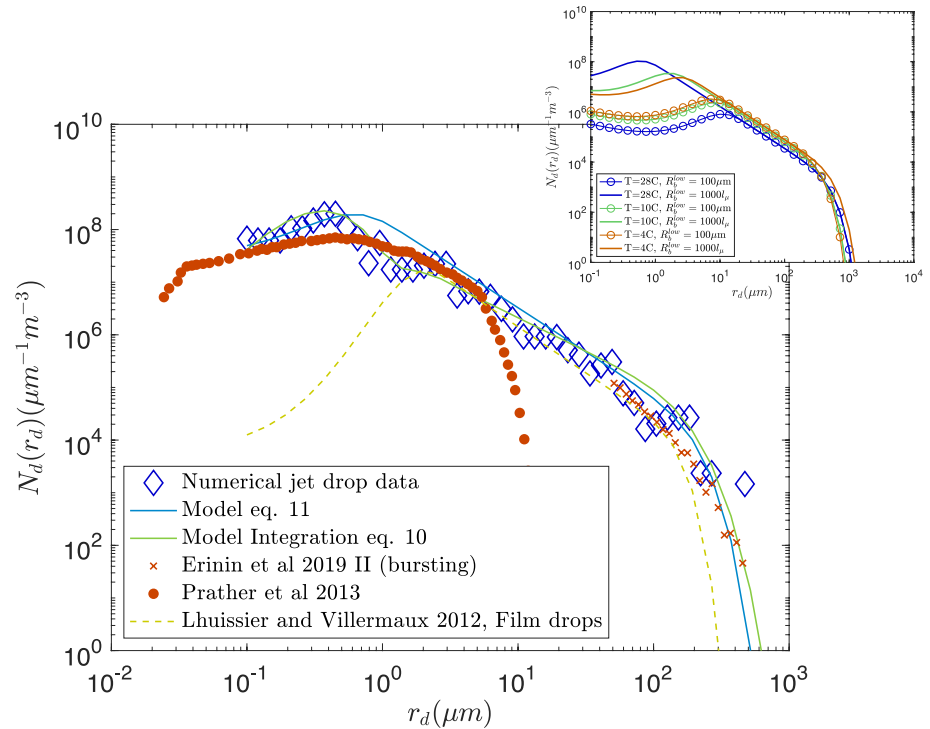


Figure 4. (a) Jet droplet size distribution due to a distribution of bubbles entrained by the breaking wave, assumed to follow the Deane and Stokes (2002) and Prather et al. (2013) bubble size distribution. We assume that all bubbles burst and produce jet drops. Blue open diamond is the predicted distribution using our modeled data. We compare the shape of the distribution with two data sets from the literature obtained for similar breaking wave conditions and bubble size distribution. Note that the vertical normalization is arbitrary as it was not provided in the experimental data sets, and so only the shape can be commented. Red dots are measurements from Prather et al. (2013) of dry aerosol. Conversion to liquid droplet size is a factor 2. Solid and dotted red are large drops measurements from Erinin et al. (2019) using holographic measurements for larger drops. (b) Sensitivity of the model jet drop distribution, given by Equation 11, for temperature from 4°C to 28°C. For each temperature, two low bubble size cut-off are considered, either 100 μm (circle lines) or $R_b^{low} = 1000\mu\text{m}$.

The bounds of integration are particularly important, as they will set the smallest and largest drop being produced. From the consideration above, we have the upper bound, say R_b^{up} which will be around 2.7 mm, which is slightly larger than the typical Hinze scale, and close to the end of the $q(R_b) \propto R_b^{-3/2}$ regime. The lower bound can be discussed in terms of the absolute smallest bubble able to produce a jet drop, $R_b^{low} / l_\mu \approx 900$, which at 28°C will be around 10 μm . However, two comments are necessary. First, measurements of the bubble size distribution under a breaking wave, or plunging waterfall used to study drop production (Deane & Stokes, 2002; Prather et al., 2013) rarely extend below 20 μm . Second, under a breaking wave in the field, a bubble below a certain size will have a rise velocity smaller than the water turbulent fluctuations, hence will not be able to rise back to the surface. This threshold is uncertain but can be estimated to be for a rise velocity of a few cm/s, that is, bubble sizes close to 100 μm . We will consider both the absolute lower threshold of 10 μm and the probably more realistic one of 100 μm in the following for discussion.

Figure 4 (main) shows the result of integration of Equation 10, using the numerical data presented in Figure 3, the bubble size distribution Equation 9 and considering $R_b^{up} = 2$ mm and $R_b^{low} = 10\mu\text{m}$. Again, for simplicity we consider the $T = 28^\circ\text{C}$ conditions for now, but other conditions can be obtained by using the appropriate visco-capillary length scale l_μ . The resulting jet drop size distribution extend from submicron drops, with a peak at 0.5 μm before falling off for smaller drops, and extend up to about 500 μm . This demonstrates the ability of the jet drop mechanism to produce a wide spectrum of aerosol sizes, reaching the submicron range.

Since we consider the absolute prefactor from (Prather et al., 2013), we can compare quantitatively the droplet size distribution. Figure 4a shows the data set from Prather et al. (2013) and they agree quantitatively

with our numerical results in the 0.5–10 μm range. We comment that film drops are also important in this range and in the data set from Prather et al. (2013) but that precise separation between the two processes will depend on the efficiency of the ejection, which might require direct measurements of the surface dynamics. Our distribution is also in good agreement with the data from Erinin et al. (2019), but we note that due to different normalizations, only the shape and range of droplets can be discussed.

The final distribution can be discussed theoretically, by considering the various scaling laws described above, which we have expressed as algebraic relationships. The mathematical construction is similar to the one proposed by Lhuissier and Villermaux (2012) for film drops, except all scalings are different and the nature of jet drop production is coming from the jet fragmentation and not the rim dynamics as it is the case for film drops. We use the scalings described above, $q(R_b) = A_b R_b^{-3/2}$, with A_b adjusted to match the distribution from Prather et al. (2013), $n(R_b) \propto R_b^{-1/3}$ Equation 6, and $\langle r_d \rangle \propto R_b^{5/4}$ Equation 7; and defining α and β such that $q(R_b)n(R_b) \propto R_b^{-\alpha}$ and $\langle r_d \rangle \propto R_b^\beta$, and introducing $\zeta = (\alpha - 1)/\beta = 2/3$, Equation 10 can be integrated yielding:

$$N_d(r_d) = \mathcal{A} r_d^{-1-\zeta} \left[\Gamma_{inc}(m + \zeta, m r_d / r_d^{up}) - \Gamma_{inc}(m + \zeta, m r_d / r_d^{low}) \right] \quad (11)$$

where $\mathcal{A} = A_b (\chi / \eta) l_\mu^{7/12}$ is nondimensional and aggregates the prefactors from the bubble size distribution, the mean drop size and average number of drops (with $(\chi / \eta) l_\mu^{7/12} \approx 0.38$ at 28°C), and Γ_{inc} is the incomplete Gamma function, $m = 4$ the order of the Gamma function for the individual bubble bursting jet drop statistics. This leads to a jet drop size distribution following $N_d(r_d) \propto r_d^{-1-\zeta} \propto r_d^{-5/3}$ between the smallest and highest drop size ejected, determined as $r_d^{low} = \langle r_d \rangle (R_b^{low}) = \eta R_b^{low 5/4} l_\mu^{-1/4}$, and similarly for the largest drop size.

The integration of Equation 10 and the final model, Equation 11, are displayed in Figure 4a and describe very well the numerical data. Note that the integration of Equation 10 uses the same bubble size resolution as the one from the numerical data (with bubble size resolved every 10 μm at small size) and therefore matches small drop behavior more closely than the final Equation 11, which would correspond to effectively a higher bubble and droplet sampling.

The same mathematical construction performed by Lhuissier and Villermaux (2012) for film drops is also shown in Figure 4a (with y-axis arbitrarily scaled). This led to $\zeta^{film} = 3/4$, so that $N_d(r_d)^{film} \propto r_d^{-7/4}$ which is slightly steeper than the jet drop distribution, between the upper and lower bound of film drop production. Film drops are produced by the retraction of the cap of the bubble, and hence need to be for bubbles $R_b \sim l_c$, the capillary length. Lhuissier and Villermaux (2012) discuss film drop production from $R_b \approx 1$ mm to $R_b \approx 10$ mm, and the corresponding mean drop size is $\langle r_d \rangle \propto R_b^{3/8} h_b^{5/8}$, where h_b is the film thickness at rupture. The film thickness at rupture is itself a function of the bubble size and lifetime, and in non-saline water, the minimal measured thickness is about 0.1–1 μm (Lhuissier & Villermaux, 2012; Néel & Villermaux, 2018; Poulain et al., 2018), leading to an estimation of the smallest liquid drop size around 1–4 μm . Note that smaller films in salt water could lead to smaller drops and evaluations of the smallest film size remains a fundamental open question (Lhuissier & Villermaux, 2012; Néel & Villermaux, 2018). Separately numerous measurements have reported solid dry particles attributed to film drops down to 0.01 μm (Cipriano & Blanchard, 1981; Cipriano et al., 1983; Mårtensson et al., 2003; Resch & Afeti, 1991; Sellegri et al., 2006; Wang et al., 2017). Below 0.1 μm , the sea spray aerosols are mainly of organic composition (Bertram et al., 2018; Quinn et al., 2015), their size not directly proportional to the liquid drop size contrary to the sea salt aerosols.

The inset of Figure 4 shows the modeled distribution Equation 11 for temperature conditions from 4°C to 28°C (i.e., various l_μ). For drops in the 10–500 μm range, the lower temperature leads to an increase in production, while the smallest drop produced depends on the choice of lower bound and temperature (through the viscosity variations). Indeed, the smallest bubble able to produce jet drop is likely to be given by the smallest bubble size able to reach the surface after a breaking wave event, which might be larger than 10 μm . Considering the rise velocity of bubbles in quiescent flow, compared to typical turbulence background velocity (Woolf & Thorpe, 1991), have argued that bubbles below 50–200 μm will fully dissolve, which would lead to a cut-off in the ocean of jet drops between 0.5 and 20 μm , depending on the water

temperature. Assuming a cut-off at 100 μm for the bubbles bursting at the ocean surface, lower temperatures lead to slightly smaller bubbles, while the opposite effect would take place if the lower bound considered is the peak of production at $R_b/l_\mu \approx 1,000$. This highlights the importance of understanding the role of temperature on the bubble size distribution, and which bubbles actually rise and burst at the ocean surface.

5. Conclusion

In this study, we quantify the size distribution of jet drops generated by bursting bubbles, initially entrained by breaking waves. We demonstrate that the mechanism of jet drop can produce a wide range of liquid droplet sizes, ranging from 0.5 μm drops produced by 10–20 μm bubbles (at 20°C), upto 500 μm drops produced by millimetric bubbles. This confirms the recent experimental discussion from Wang et al. (2017), which demonstrated that both film and jet drops can produce submicrons aerosols, with different chemical compositions. The relative importance of film and jet drops remains to be better quantified, and will likely depend on the physico-chemical conditions of the water, including water temperature, humidity conditions, and contamination, which will affect the film drainage process and the properties of the resulting film drops. The lower bound of bubble size for jet drop production is shown to depend on water viscosity, through the visco-capillary length. However, we note that submicrons drops result from bubbles in the 10–50 μm range which might not rise to the ocean surface in the field. The characterization of the surface bubble size distribution in the field would bring invaluable data to clarify this question. The proposed formulations present a natural dependency on temperature, through their dependency on water viscosity, but do not account for other physico-chemical effects, such as surfactants, and neglect any collective behavior at the water surface.

Data Availability Statement

All data used in preparing this work are publicly available at <http://arks.princeton.edu/ark:/88435/dsp018623j1807>. The Basilisk library is available at: <http://basilisk.fr>, and the simulation file for the bursting simulation is available at <http://basilisk.fr/sandbox/aberny/README#the-general-case>.

Acknowledgments

This work was supported by the National Science Foundation under Grant No. 1849762 to L. Deike, and the Cooperative Institute for Modeling the Earth's System at Princeton University.

References

- Berny, A., Deike, L., Séon, T., & Popinet, S. (2020). Role of all jet drops in mass transfer from bursting bubbles. *Physical Review Fluids*, 5, 033605. <https://doi.org/10.1103/physrevfluids.5.033605>
- Bertram, T. H., Cochran, R. E., Grassian, V. H., & Stone, E. A. (2018). Sea spray aerosol chemical composition: Elemental and molecular mimics for laboratory studies of heterogeneous and multiphase reactions. *Chemical Society Reviews*, 47, 2374–2400. <https://doi.org/10.1039/c7cs00008a>
- Blanchard, D. C. (1954). Bursting of bubbles at an air-water interface. *Nature*, 173. <https://doi.org/10.1038/1731048a0>
- Blanchard, D. C., & Woodcock, A. H. (1957). Bubble formation and modification in the sea and its meteorological significance. *Tellus*, 9, 145–158. <https://doi.org/10.1111/j.2153-3490.1957.tb01867.x>
- Blanco-Rodríguez, F. J., & Gordillo, J. (2020). On the sea spray aerosol originated from bubble bursting jets. *Journal of Fluid Mechanics*, 886. <https://doi.org/10.1017/jfm.2019.1061>
- Blenkinsopp, C. E., & Chaplin, J. R. (2010). Bubble size measurements in breaking waves using optical fiber phase detection probes. *IEEE Journal of Oceanic Engineering*, 35, 388–401. <https://doi.org/10.1109/joe.2010.2044940>
- Brasz, C. F., Bartlett, C. T., Walls, P. L. L., Flynn, E. G., Yu, Y. E., & Bird, J. C. (2018). Minimum size for the top jet drop from a bursting bubble. *Physical Review Fluids*, 3. <https://doi.org/10.1103/PhysRevFluids.3.074001>
- Cipriano, R. J., & Blanchard, D. C. (1981). Bubble and aerosol spectra produced by a laboratory “breaking wave”. *Journal of Geophysical Research*, 86, 8085–8092. <https://doi.org/10.1029/jc086ic09p08085>
- Cipriano, R. J., Blanchard, D. C., Hogan, A. W., & Lala, G. G. (1983). On the production of aiten nuclei from breaking waves and their role in the atmosphere. *Journal of the Atmospheric Sciences*, 40, 469–479. [https://doi.org/10.1175/1520-0469\(1983\)040<0469:otpoan>2.0.co;2](https://doi.org/10.1175/1520-0469(1983)040<0469:otpoan>2.0.co;2)
- Cochran, R. E., Ryder, O. S., Grassian, V. H., & Prather, K. A. (2017). Sea spray aerosol: The chemical link between the oceans, atmosphere, and climate. *Accounts of Chemical Research*, 50, 599–604. <https://doi.org/10.1021/acs.accounts.6b00603>
- Deane, G. B., & Stokes, M. D. (2002). Scale dependence of bubble creation mechanisms in breaking waves. *Nature*, 418(6900), 839–844. <https://doi.org/10.1038/nature00967>
- Deike, L., Ghabache, E., Liger-Belair, G., Das, A. K., Zaleski, S., Popinet, S., & Seon, T. (2018). The dynamics of jets produced by bursting bubbles. *Physical Review Fluids*, 3. <https://doi.org/10.1103/physrevfluids.3.013603>
- Deike, L., Lenain, L., & Melville, W. K. (2017). Air entrainment by breaking waves. *Geophysical Research Letters*, 44(8), 3779–3787. <https://doi.org/10.1002/2017gl072883>
- Deike, L., & Melville, W. K. (2018). Gas transfer by breaking waves. *Geophysical Research Letters*, 45, 10–482. <https://doi.org/10.1029/2018gl078758>
- Deike, L., Melville, W. K., & Popinet, S. (2016). Air entrainment and bubble statistics in breaking waves. *Journal of Fluid Mechanics*, 801, 91–129. <https://doi.org/10.1017/jfm.2016.372>
- de Leeuw, G., Andreas, E. L., Anguelova, M. D., Fairall, C. W., Lewis, E. R., O’Dowd, C., et al. (2011). Production flux of sea spray aerosol. *Reviews of Geophysics*, 49. <https://doi.org/10.1029/2010rg000349>

- Duchemin, L., Popinet, S., Josserand, C., & Zaleski, S. (2002). Jet formation in bubbles bursting at a free surface. *Physics of Fluids*, *14*(9), 3000–3008. <https://doi.org/10.1063/1.1494072>
- Erinin, M. A., Wang, S. D., Liu, R., Towle, D., Liu, X., & Duncan, J. H. (2019). Spray generation by a plunging breaker. *Geophysical Research Letters*, *46*, 8244–8251. <https://doi.org/10.1029/2019gl082831>
- Gañán-Calvo, A. M. (2017). Revision of bubble bursting: Universal scaling laws of top jet drop size and speed. *Physical Review Letters*, *119*(20), 204502. <https://doi.org/10.1103/physrevlett.119.204502>
- Garrett, C., Li, M., & Farmer, D. (2000). The connection between bubble size spectra and energy dissipation rates in the upper ocean. *Journal of Physical Oceanography*, *30*, 2163–2171. [https://doi.org/10.1175/1520-0485\(2000\)030<2163:tcbbs>2.0.co;2](https://doi.org/10.1175/1520-0485(2000)030<2163:tcbbs>2.0.co;2)
- Ghabache, E. (2015). *Surface libre hors équilibre: De l'effondrement de cavité aux jets étirés* (Unpublished doctoral dissertation)
- Ghabache, E., Antkowiak, A., Josserand, C., & Séon, T. (2014). On the physics of fizziness: How bubble bursting controls droplets ejection. *Physics of Fluids*, *26*. <https://doi.org/10.1063/1.4902820>
- Ghabache, E., Liger-Belair, G., Antkowiak, A., & Séon, T. (2016). Evaporation of droplets in a champagne wine aerosol. *Scientific Reports*, *6*, 25148. <https://doi.org/10.1038/srep25148>
- Ghabache, E., & Séon, T. (2016). Size of the top jet drop produced by bubble bursting. *Physical Review Fluids*, *1*, 051901. <https://doi.org/10.1103/physrevfluids.1.051901>
- Gordillo, J. M., & Rodríguez-Rodríguez, J. (2019). Capillary waves control the ejection of bubble bursting jets. *Journal of Fluid Mechanics*, *867*, 556–571. <https://doi.org/10.1017/jfm.2019.161>
- Hinze, J. O. (1955). Fundamentals of the hydrodynamic mechanism of splitting in dispersion processes. *AIChE Journal*, *1*, 289–295. <https://doi.org/10.1002/aic.690010303>
- Lai, C.-Y., Eggers, J., & Deike, L. (2018). Bubble bursting: Universal cavity and jet profiles. *Physical Review Letters*, *121*(14), 144501. <https://doi.org/10.1103/physrevlett.121.144501>
- Lewis, E. R., & Schwartz, S. E. (2004). *Sea salt aerosol production. mechanisms, methods, measurements, and models*. Washington DC: American Geophysical Union. <https://doi.org/10.1029/gm152>
- Lhuissier, H., & Villermaux, E. (2012). Bursting bubble aerosols. *Journal of Fluid Mechanics*, *696*, 5–44. <https://doi.org/10.1017/jfm.2011.418>
- Mårtensson, E., Nilsson, E., de Leeuw, G., Cohen, L., & Hansson, H.-C. (2003). Laboratory simulations and parameterization of the primary marine aerosol production. *Journal of Geophysical Research*, *108*(D9). <https://doi.org/10.1029/2002jd002263>
- Mostert, W., & Deike, L. (2020). Inertial energy dissipation in shallow-water breaking waves. *Journal of Fluid Mechanics*, *890*. <https://doi.org/10.1017/jfm.2020.83>
- Mostert, W., Popinet, S., & Deike, L. (2021). High-resolution direct simulation of deep water breaking waves: Transition to turbulence, bubbles and droplets production, 43. Submitted. Retrieved from <https://arxiv.org/pdf/2103.05851.pdf>
- Mueller, J. A., & Veron, F. (2014). Impact of sea spray on air-sea fluxes. part ii: Feedback effects. *Journal of Physical Oceanography*, *44*, 2835–2853. <https://doi.org/10.1175/jpo-d-13-0246.1>
- Neel, B., & Deike, L. (2021). Collective surface bubbles dynamics and bursting, and the role of surface contamination. *Journal of Fluid Mechanics*, *917*(A46). <https://doi.org/10.1017/jfm.2021.272>
- Néel, B., & Villermaux, E. (2018). The spontaneous puncture of thick liquid films. *Journal of Fluid Mechanics*, *838*, 192–221. <https://doi.org/10.1017/jfm.2017.877>
- Ortiz-Suslow, D. G., Haus, B. K., Mehta, S., & Laxague, N. J. M. (2016). Sea spray generation in very high winds. *Journal of the Atmospheric Sciences*, *73*, 3975–3995. <https://doi.org/10.1175/jas-d-15-0249.1>
- Peng, T., & Richter, D. (2020). Influences of polydisperse sea spray size distributions on model predictions of air-sea heat fluxes. *Journal of Geophysical Research: Atmospheres*, *125*, e2019JD032326. <https://doi.org/10.1029/2019jd032326>
- Popinet, S. (2009). An accurate adaptive solver for surface-tension-driven interfacial flows. *Journal of Computational Physics*, *228*, 5838–5866. <https://doi.org/10.1016/j.jcp.2009.04.042>
- Popinet, S. (2018). Numerical models of surface tension. *Annual Review of Fluid Mechanics*, *50*, 49–75. <https://doi.org/10.1146/annurev-fluid-122316-045034>
- Poullain, S., Villermaux, E., & Bourouiba, L. (2018). Ageing and burst of surface bubbles. *Journal of Fluid Mechanics*, *851*, 636–671. <https://doi.org/10.1017/jfm.2018.471>
- Prather, K. A., Bertram, T. H., Grassian, V. H., Deane, G. B., Stokes, M. D., DeMott, P. J., et al. (2013). Bringing the ocean into the laboratory to probe the chemical complexity of sea spray aerosol. *Proceedings of the National Academy of Sciences*, *110*, 7550–7555. <https://doi.org/10.1073/pnas.1300262110>
- Quinn, P. K., Collins, D. B., Grassian, V. H., Prather, K. A., & Bates, T. S. (2015). Chemistry and related properties of freshly emitted sea spray aerosol. *Chemical Reviews*, *115*, 4383–4399. <https://doi.org/10.1021/cr500713g>
- Resch, F., & Afeti, G. (1991). Film drop distributions from bubbles bursting in seawater. *Journal of Geophysical Research*, *96*, 10681–10688. <https://doi.org/10.1029/91jc00433>
- Rivière, A., Mostert, W., Perrard, S., & Deike, L. (2021). Sub-hinze scale bubble production in turbulent bubble break-up. *Journal of Fluid Mechanics*, *917*(A40). <https://doi.org/10.1017/jfm.2021.243>
- Rojas, G., & Loewen, M. R. (2007). Fiber-optic probe measurements of void fraction and bubble size distributions beneath breaking waves. *Experiments in Fluids*, *43*, 895–906. <https://doi.org/10.1007/s00348-007-0356-5>
- Sellegrì, K., O'Dowd, C., Yoon, Y., Jennings, S., & de Leeuw, G. (2006). Surfactants and submicron sea spray generation. *Journal of Geophysical Research*, *111*. <https://doi.org/10.1029/2005jd006658>
- Spiel, D. E. (1994). The number and size of jet drops produced by air bubbles bursting on a fresh water surface. *Journal of Geophysical Research*, *99*, 10289–10296. <https://doi.org/10.1029/94jc00382>
- Spiel, D. E. (1997). More on the births of jet drops from bubbles bursting on seawater surfaces. *Journal of Geophysical Research*, *102*, 5815–5821. <https://doi.org/10.1029/96jc03582>
- Tang, I. N., Tridico, A. C., & Fung, K. H. (1997). Thermodynamic and optical properties of sea salt aerosols. *Journal of Geophysical Research*, *102*, 23269–23275. <https://doi.org/10.1029/97jd01806>
- Toba, Y. (1959). Drop production by bursting of air bubbles on the sea surface (ii) theoretical study on the shape of floating bubbles. *Journal of the Oceanographical Society of Japan*, *15*, 121–130. <https://doi.org/10.5928/kaiyou1942.15.121>
- Troitskaya, Y., Kandaurov, A., Ermakova, O., Kozlov, D., Sergeev, D., & Zilitinkevich, S. (2018). The “bag breakup” spume droplet generation mechanism at high winds. part I: Spray generation function. *Journal of Physical Oceanography*, *48*, 2167–2188. <https://doi.org/10.1175/jpo-d-17-0104.1>

- van Hooft, J. A., Popinet, S., van Heerwaarden, C. C., van der Linden, S. J. A., de Roode, S. R., & van de Wiel, B. J. H. (2018). Towards adaptive grids for atmospheric boundary-layer simulations. *Boundary-Layer Meteorology*, *167*, 421–443. <https://doi.org/10.1007/s10546-018-0335-9>
- Veron, F. (2015). Ocean spray. *Annual Review of Fluid Mechanics*, *47*, 507–538. <https://doi.org/10.1146/annurev-fluid-010814-014651>
- Veron, F., Hopkins, C., Harrison, E., & Mueller, J. (2012). Sea spray spume droplet production in high wind speeds. *Geophysical Research Letters*, *39*. <https://doi.org/10.1029/2012gl052603>
- Villermaux, E. (2020). Fragmentation versus cohesion. *Journal of Fluid Mechanics*, *898*. <https://doi.org/10.1017/jfm.2020.366>
- Wang, X., Deane, G. B., Moore, K. A., Ryder, O. S., Stokes, M. D., Beall, C. M., et al. (2017). The role of jet and film drops in controlling the mixing state of submicron sea spray aerosol particles. *Proceedings of the National Academy of Sciences*, *114*. <https://doi.org/10.1073/pnas.1702420114>
- Woolf, D. K., & Thorpe, S. A. (1991). Bubbles and the air-sea exchange of gases in near-saturation conditions. *Journal of Marine Research*, *49*, 435–466. <https://doi.org/10.1357/002224091784995765>